

## **Robustness of biometric wood log traceability using digital log end images**

R. Schraml    J. Charwat-Pessler<sup>a</sup>    A. Petutschnigg<sup>a</sup>    A. Uhl

<sup>a</sup>University of Applied Sciences Salzburg, Markt 136a, 5431 Kuchl, Austria

Technical Report 2014-08

December 2014

### **Department of Computer Sciences**

Jakob-Haringer-Straße 2  
5020 Salzburg  
Austria  
[www.cosy.sbg.ac.at](http://www.cosy.sbg.ac.at)

**Technical Report Series**

# Robustness of biometric wood log traceability using digital log end images <sup>☆</sup>

R. Schraml<sup>a,\*</sup>, J. Charwat-Pessler<sup>b,\*</sup>, A. Petutschnigg<sup>b</sup>, A. Uhl<sup>a</sup>

<sup>a</sup>University of Salzburg, Jakob Haringer Str. 2, 5020 Salzburg, Austria

<sup>b</sup>University of Applied Sciences Salzburg, Markt 136a, 5431 Kuchl, Austria

---

## Abstract

Log traceability in the timber based industries is a basic requirement to fulfill economical, social and legal requirements. This work introduces into biometric log recognition using digital log end images and investigates the robustness to real world log end cross-section (CS) variations. In order to investigate longitudinal and surface CS variations three tree logs were sliced and captured in different sessions. Equal as in our initial study [19] a technique closely related to feature-based fingerprint matching is used to compute biometric templates and in addition three matching procedures are utilized to compute matching scores between CS images. On this basis, our experiments enable to present first fundamental insights and constraints on the robustness and general applicability of biometric log recognition using log end images to identify logs in an industrial application. Our results for different identification performance scenarios indicate that the matching procedure which is based on annual ring pattern and shape information is robust to log length cutting using different cutting tools. By showing up the potentials and basic requirements this study is of major importance and contributes to the further development of a biometric log recognition system.

**Keywords:** Biometric log traceability, Log tracking, Cross-section analysis, Log end face analysis, European Timber Regulation, Chain of Custody, Forest sustainability assessment

---

## 1. Introduction

Many efforts had been made in the past in order to assess illegal logging, its associated causes and how such actions could be effectively disabled in future. Besides corruption on different governmental authority levels and land reclamation for requirements such as mining, plantations or agriculture, illegal logging is known to be one of the main driving forces promoting deforestation [18, 21, 15]. It is a phenomenon comprising timber harvesting, timber trade and disposal occurring around the world and affects biodiversity, hydrological cycles and contributes considerably soil erosion.

These problems were officially addressed at the UN Conference on Environment and Development (UNCED) held in Rio de Janeiro in 1992 and consequently a document called Agenda 21 was concluded, providing voluntary commitments on sustainable forest management and development and offering a basis for non-governmental, independent forest certification [23]. According to a report supported by the World Bank, illegal logging is considered ten years later still as a major threat to environment being closely linked to political, social and economical conditions and therefore emphasizing the need for effective traceability methods within the wood supply chain [3].

Efforts in fighting illegal logging on the EU level led to the Forest Law Enforcement Governance and Trade Action Plan (FLEGT) defined in 2003 and the EU Timber Regulation (EUTR) prohibiting the placement of illegally harvested timber and wood products derived there from. This regulation, initially proposed by the Commission in 2008, is legally binding on all EU member states, each being responsible for national implementation and has come into force since march 2013. This regulation claims traceability of timber and timber products throughout the supply chain providing information on operators, traders and, if possible, of retailers [4].

Traceability of timber and wood products is generally expected to restrict illegal logging and is supposed to be to the beneficial of companies and consumers [22]. In fact empirical information on quantities and linkages of internationally traded wood are indispensable in order to assess causal relationships for illegal logging and to take effective steps preventing deforestation in future [13]. Admittedly landsat data on forest resources may considerably vary from official data collection, there-from an improved monitoring is highly required in order to gain reliable information [15]. A contemporary managed database in conjunction with wood labelling would certainly provide such a basis and thus impede illegal logging, fraud and misuse in future.

A wide range of log traceability systems are applied in order to identify and track logs in the past, each method showing limitations due to costs, practical implementation or weather conditions. The applications range from punching, coloring or barcoding log ends to more recently developed techniques as DNA fingerprinting and usage of RFID transponders [22].

---

<sup>☆</sup>This work is partially funded by the Austrian Science Fund (FWF) under Project No. TRP-254.

<sup>☆☆</sup>Cross Section (CS), Matching Score (MS), Score Distribution (SD), No Knots (NK), Slice Distance Group (SDG)

\*Corresponding authors

Email addresses: rschraml@cosy.sbg.ac.at (R. Schraml), johann.charwat-pessler@fh-salzburg.ac.at (J. Charwat-Pessler)

Another approach comes down to track logs using biometric log characteristics. Investigations on the hypothesis that logs are separate entities on the basis of biometric log characteristics were presented in the works of [1, 2, 5, 6, 7], which show up the high potential of biometric log recognition. The approaches presented in [1, 2, 6] utilized 2D and 3D scanners to extract geometric wood properties. In [5, 7] a computer tomography scanner was used to extract knot positions to enable traceability between logs and the cut boards. Because of low recognition rates, these approaches are not applicable for industrial usage and are less suitable to deal with the increasing variety of trees at forest site. Additionally, the utilized capturing devices are expensive and not applicable in the forest based industries.

On account of the fact, that timber offers characteristics on log end faces in terms of annual rings, pith position, shape and dimension it is assumed that cross-section images of log ends can be used as biometric characteristic for log identification. Images containing a cross-section (CS) of a wood log are denoted as cross-section images (CS-Images) throughout this work.

This study introduces the concept of biometric log recognition using log end images and elaborates the robustness to practical issues of an industrial application. In case of CS-Images of log ends, CS variations are pretty unpredictable and the biometric system must be able to identify a single wood log based on two different CS-Images in which the CSs of the same log show up strong variations. Consequently, the applicability of biometric log recognition using log end images depends significantly on the robustness to CS variations which arise in an industrial application. Basically, the biometric system must discriminate between CS-Images of the same log and CS-Images of different logs. Thereby, a high variability between CS-Images of the same log end deteriorates the discriminative power of the biometric system.

Two types of variations which arise in an industrial application are: Temporal and Longitudinal variations of cross-sections (CSs). Temporal variations are caused by light, humidity and other environmental influences and result in deformations like cracks and discolorations. Longitudinal variations result from log end cutting in the sawmill or from capturing different log ends. In [19] first investigations on temporal and longitudinal variations based on time-delay captured CS-Images of 35 Slices of a single log were presented.

Equal as in [19] the FingerCode approach [11, 9] is adopted to CS-Images. By introducing three matching procedures this study additionally elaborates the strength of the annual ring pattern and the CS shape as biometric feature. In addition to the single log used in [19], further two logs are used for the experimental evaluation of this study. From each log 16 Slices were cut down and the rough and sanded CS surfaces of each slice were captured with a digital camera. Consequently, the captured CS-Images enable to consider a third group of CS variations which we denote as surface variations. Additionally, interclass matching scores (MSs) between the CS-Images of three different tree logs are computed.

Based on CS-Images of three logs, this work contributes to the development of biometric log recognition in assessing two

main objectives in the experiments. The first objective is to investigate the separability between intra- and interclass MSs. For this purpose, the verification performance of the biometric system is evaluated. Furthermore, detailed investigations on the impact of surface and longitudinal variations to the intra-class variability and the separability of the interclass MSs are presented. Thereby it is assessed if the CS surface has an impact on the longitudinal variations of each log. For this purpose, the longitudinal MSs of the rough and sanded slices from both logs are evaluated and the results are compared to the longitudinal MSs computed in [19]. In comparing the interclass MSs of three logs to the surface and longitudinal MSs it is possible to draw fundamental conclusions on the robustness and applicability of biometric log recognition using log end images.

Second, first investigations on the identification performance of biometric log recognition using log end images are presented. Introductory, general assertions about the impact of surface and longitudinal variations on the identification performance are presented. Subsequently, identification rates for different scenarios are presented. For these scenarios, it is assumed that the log is length cut in the sawmill. Thereby, the first cut in the forest and the second cut in the sawmill can be performed with different cutting tools. This results in a mixture of surface and longitudinal variations. Furthermore, it is assessed to which extent the identification rates are influenced by the width of the piece which is cut-off from the log end.

At, first Section 2 introduces the computation and matching of biometric templates from CS-Images using Gabor-based features. The experimental setup and results are presented in Section 2.4 followed by the conclusion in Section 4.

## 2. Materials and Methods

By superficially comparing the patterns of human fingerprints to annual ring patterns of wood log ends one finds that these are closely resembling to each other. Human fingerprint recognition is well-investigated and there exist three mainly used groups of approaches: Minutiae-based, Correlation-based and Feature-based approaches [16]. Apart from the presence of the pith as detectable feature, CS patterns do not exhibit further constant features like minutia's in fingerprints. Hence, minutiae-based approaches are not qualified for log CSs.

Basically, the scheme of a biometric recognition system is set up on five components: Data acquisition, Preprocessing, Feature Extraction, Template Generation and Template Matching. In case of biometric log recognition using log end images, data acquisition is the capturing of digital CS-Images of log ends. In the preprocessing stage the CS in the CS-Image is separated from the background, aligned and subsequently the CS is enhanced. Due to the ability of feature-based methods to capture information of the fingerprint ridge pattern they can be extended to work with CS patterns. For this purpose, we have adopted the texture feature-based FingerCode approach by [11], [9] to extract features from CS-Images. The extracted features of a CS-Image are stored in a vector which is denoted as cross-section code (CS-Code). A template of a CS-Image incorporates a set

of CS-Codes which are computed for differently rotated versions of the CS-Image.

Finally, template matching is the task of verification or identification of an individual or subject. For this purpose, the individual/ subject must be enrolled in the biometric system. In case of log recognition, the enrolment procedure could be performed during the harvesting procedure in the forest. An exemplary enrolment scheme for wood logs is depicted in Fig. 2. For enrolment the end of a fresh cut log is captured using a

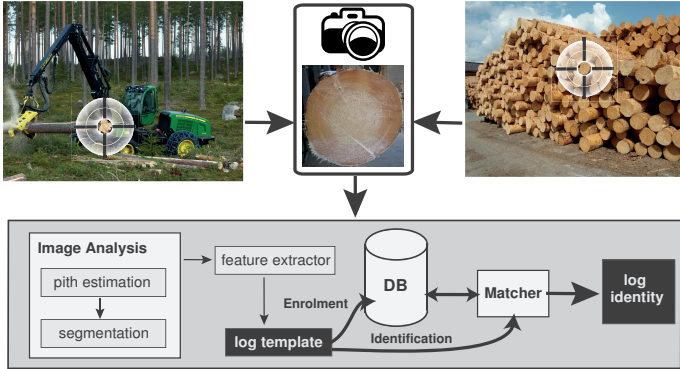


Figure 1: Exemplary enrolment and identification schemes for a biometric log recognition system. The enrolment can be done in the forest using a digital camera mounted on a harvester.

digital camera mounted on a harvester. Subsequently, the first four steps of the biometric system chain are completed and the computed log template is stored to a database. Additionally, the harvester operator can assign further informational meta data to each log template in the database.

In case of wood logs, recognition is related to the identification of each log. An exemplary identification scheme in the sawmill environment is shown in 2. Basically, images of log ends can be captured at each stage of the log processing chain. In the sawmill the ends of a log are conveniently cut again. This leads to a clean CS surface and aids the quality assessment of each log. CS-Images for identification could be captured at the sorting station, at the sawmill yard or at any conveyor belt equipped with a capturing device. Subsequently, the CS-Image is processed by the biometric system and a log template is computed. This log template is matched to all available log templates in the database. Commonly, the best match is used to determine the identity of the log. Furthermore, additional meta data can be retrieved or appended from/ to the log record in the database.

In the next three sections a detailed introduction on pre-processing (Section 2.1), CS-Code computation (Section 2.2) and three matching procedures (Section 2.3) between two CS-Codes is given. Finally, in the last Section 2.4 basics for the experimental evaluation are introduced.

### 2.1. Cross-section registration & enhancement

Due to the cutting pattern annual ring enhancement is a crucial task for any subsequent feature extraction procedure. As opposed to human fingerprints, the frequency of the annual ring pattern is strongly varying. Our enhancement procedure

is based on the fingerprint enhancement approach presented in [8]. CS registration is performed in three steps. The left image in Fig. 2 shows an example for an input CS-Image. The CS border and the pith position have to be determined in advance (see [20],[17]). For image registration the image is rotated around the pith position, cropped to the CS bounding box and finally scaled to 512 pixels in width. Rotation can be performed to generate rotated versions of each CS-Image or to align the CS to a unique position (e.g. according to the center of mass). For CS-Image enhancement the CS is subdivided in half/ non-overlapping blocks (eg. 16x16 pixels). Enhancement is performed in three consecutive stages: Local orientation estimation, local frequency estimation and adaptive filtering.

At first, for each block principal component analysis of the local Fourier Spectrum is performed to determine its local orientation (see [20]). Commonly, CSs are disturbed due to cutting. Thus, wrong orientations are slightly corrected by low-pass filtering the local orientation field with a Gaussian filter. Next, for each block and its local orientation the dominant frequency is determined. For this purpose, the local Fourier Spectrum of each block is subdivided into subbands and sectors. The dominating frequency of a block is determined by summing up all frequency magnitudes in each sector subband. It is assumed that the maximum sector-subband represents the dominating frequency. If the maximum sector does not correspond to the block orientation the result is neglected. In a further step for each neglected value the local frequency is interpolated using a Gaussian filter.

In the filtering stage the Fourier Spectrum of each block is filtered with a Log-Gabor (introduced by [14]) which is tuned to its local orientation and frequency. Furthermore, experiments showed that a bandwidth of three times the variance of the Fourier Spectrum and as spread value the blocksize/4 are well suited for filtering. By using the fast inverse Fourier transform the filtered Fourier Spectra are utilized as new block values. Boundary effects are reduced by using half-overlapping blocks. An exemplary result of the registration & enhancement procedure is depicted in Fig. 2.

### 2.2. Cross-section code computation

The CS-Code computation is based on the FingerCode approach proposed in [11] and [9]. This technique utilizes a Gabor-based descriptor which extracts local ridge orientations of a fingerprint. Because of the constant ridge frequencies in human fingerprints a single Gabor filter and its rotated versions are sufficient. The frequencies of annual ring patterns are strongly varying and thus different Gabor filters are required to capture additional information from the annual ring frequencies in different orientations. For a CS image width of 512 pixels six different Gabor filters are suggested. For each Gabor filter eight rotated versions are created. Consequently, the Gabor filterbank consists of 48 filters.

The CS-Code computation is performed in three stages. In the first stage the enhanced input image is filtered with each filter in the filterbank. Each filtered image is subdivided into blocks (e.g. 32x32 pixels). For all blocks the absolute deviations of the gray values are computed. The absolute devia-

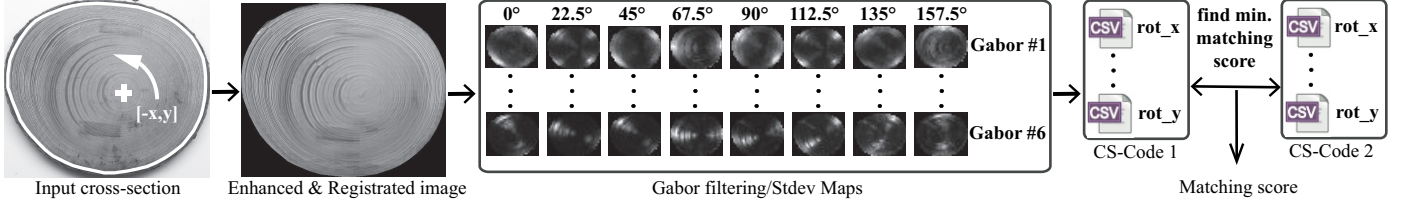


Figure 2: CS-Code computation and matching scheme

tions of each image are stored into a matrix, which can be denoted as Standard Deviation Map (Stdev Map). In the middle of Fig. 2, the filtering and Stdev map computation procedure is illustrated. Altogether 48 Stdev Maps are computed and stored as one-dimensional vectors in a CSV file. For each value of a single Stdev map which is not within the CS border a marker value (e.g. -1) is stored into the CSV file which is relevant for the matching procedure. Rotational variances are compensated by repeatedly computing features for rotated versions of the input CS-Image. Compared to fingerprints, the rotational misalignment range of a CS-Image is not restricted to a certain range. One strategy to solve this issue, is to perform rotational pre-alignment in the registration and enhancement stage to restrict the misalignment range.

### 2.3. Cross-section code matching

The matching between two different CS-Images is performed by computing the minimum matching score between all CS-Codes from both CS-Images. The score between the feature values of two CS-Codes ( $CS_1, CS_2$ ) can be computed with a set of distance metrics ( $D$ ). In this work the Manhattan distance is utilized. Basically, the MS between two CS-Codes is defined as:

$$MS(CS_1, CS_2) = \frac{1}{M} \sum_{i=0}^N D(CS_1(i), CS_2(i)) \quad (1)$$

where  $CS_1, CS_2$  are two feature vectors of the CS-Codes which are compared,  $i$  specifies the index of the feature value in both vectors.

As noted in Section 2.2, background feature values are specified by a certain marker. These markers specify the shape of the CS and the matching procedure can utilize or ignore this information. We define  $MCS_1$  and  $MCS_2$  as two masks which allow to differentiate between background and CS. In contrast to fingerprints where the shapes are commonly not utilized, the CS shape is obviously a biometric feature itself. By investigating three different matching procedures the impact of incorporating shape information on the biometric system performance is evaluated. The first procedure is analogous to the Fingercodex matching procedure in [11]. Just the CS-Code feature value pairs which are in the intersection of both CSs are utilized for computing the MS. The computed MS is normalized by the amount of considered feature value pairs:  $M = |MCS_1 \cap MCS_2|$ . Consequently, this procedure just makes use of the annual ring texture as biometric feature and the MS shows up the discriminative power of the annual ring pattern. For simplicity this procedure is denoted as annual ring pattern

MS ( $MS_{AP}$ ) and the utilized distance function is given by:

$$D_{AP} = \begin{cases} |CS_1(i) - CS_2(i)| & \text{if } i \in MCS_1 \cap MCS_2 \\ 0 & \text{otherwise} \end{cases} \quad (2)$$

The second procedure ( $MS_{AP\&S}$ ) uses a distance function ( $D_{AP\&S}$ ) where a penalty value ( $P_{AP\&S}$ ) is added to all ( $(CS_1(i), CS_2(i))$ ) feature value pairs which are in the symmetric difference of the CS masks (see Eq. 3). For normalization  $M = |MCS_1 \cup MCS_2| + |MCS_1 \Delta MCS_2|$  is used. In doing this, the MS additionally increases for differently shaped CSs. For the selection of  $P_{AP\&S}$  the mean value of the feature value distributions of both CS-Codes is utilized. Consequently, the increase of the distance does not overemphasize small shape differences or small misalignments.

$$D_{AP\&S} = \begin{cases} |CS_1(i) - CS_2(i)| + P_{AP\&S} & \text{if } i \in MCS_1 \Delta MCS_2 \\ |CS_1(i) - CS_2(i)| & \text{if } i \in MCS_1 \cap MCS_2 \\ 0 & \text{otherwise} \end{cases} \quad (3)$$

The third procedure ( $MS_{AP,F}$ ) is based on score level fusion [12, p.225] of two independently computed scores. As first score the  $MS_{AP}$  score is utilized. Second the False Negative Rate (F) is computed for the shapes of the compared CSs ( $MCS_1, MCS_2$ ).

$$F = \frac{MCS_1 \Delta MCS_2}{\min(|MCS_1|, |MCS_2|)} \quad (4)$$

Finally, both scores are combined with different scaling factors (see Eq. 5). The factors are determined by considering the value ranges of both features. For this work the scaling  $\sigma_{AP}$  and  $\sigma_F$  are chosen so that the scores of both features are weighted equally.

$$MS_{AP,F} = MS_{AP} \cdot \sigma_{AP} + F \cdot \sigma_F \quad (5)$$

## 2.4. Experimental setup

### 2.4.1. Testset

The experimental evaluation is based on cross-section slices (CS-Slices) from three different European spruce logs (Log 1 - L1, Log 2 - L2, Log 3 - L3). For L1 and L2, a section of 40 centimetres was cut into 16 CS-Slices. The CS-Slices were cut with a bandsaw and the thickness of each CS-Slice is approximately 2.5 centimetres. Thereby, the sections of L1 and L2 were showing a diameter of around 230 mm and 290 mm respectively.

Subsequently, just one surface of each CS-Slice was captured two times (Nikon D90). The first CS-Image was taken from the fresh cut CS-Slices. For the second CS-Image, the surfaces of the CS-Slices were polished using a sandpaper (P 150). In the first row of Fig. 3 the two captured CS-Images of one CS-Slice of L1 and L2 are depicted.

Additionally, 35 CS-Slices from L3 are utilized in the experiments to increase the amount of MSs computed between CS-Slices from different tree logs. These CS-Slices were already used for the experiments presented in [19]. These CS-Slices were also cut with a bandsaw and their thickness accounts approximately two centimetres. From each CS-Slice four CS-Images were captured (Canon EOS 5D Mark II) with different time spans between each capturing session. Additionally,

Log	# CS-Slices	# CS-Images	Illustration
Log 1 - L1	16	2 (Rough&Sanded)	Fig. 3a
Log 2 - L2	16	2 (Rough&Sanded)	Fig. 3b
Log 3 - L3	35	4 (Time delay)	Fig. 4

Table 1: Testset overview

for each CS-Image the pith position and the border of the CS (CS-Border) were determined manually and are utilized for CS registration and computing the F-Measure in the experiments. The CS-Images in Fig. 3 illustrate the preprocessing steps for the CS-Images of CS-Slice L1 #2, L2 #10. In the first row the original images are depicted. The second and third row show the registered and enhanced versions of the CS-Images, respectively. The four time-delay captured CS-Images of CS-Slice #10 of L3 are depicted in Fig. 4.

*CS-Code computation.* Due to the fact, that the CS-Slices were not equally aligned in rotation for each CS-Image of a CS-Slice 360 CS-Codes ( $rot_{-180}, \dots, rot_0, \dots, rot_{179}$ ) are computed. Although the expected misalignment range is much smaller, CS-Codes for all rotations are computed and used for matching. Hence, it can be evaluated if there exist rotated versions of two CS-Slice images from different tree logs which are incidentally similar to each other. For registration and enhancement the rotated CSs are scaled to 512 pixels in width. The enhancement procedure is performed using 32x32 half-overlapping pixel blocks. The CS-Codes are computed using 16x16 non-overlapping blocks for the Stdev maps. The utilized Gabor filterbank is build up on six different Gabor filters tuned to 8 directions:

$$G(\lambda, \theta, \sigma, \gamma) = G(\lambda, \sigma) = ((2.5, 2), (2.5, 2), (3.5, 3), (4.5, 3), (5.5, 3), (6.5, 3)), \\ \theta = \{0, 22.5, \dots, 135, 157.5\}, \gamma = 0.7$$

#### 2.4.2. Evaluation background

Before presenting the results, relevant basics for the experimental evaluation are introduced. First, a short introduction on biometric performance evaluation is presented. Subsequently, three types of wood log CS variations are defined and the construction of the intra- and interclass score distributions (SDs) used in the evaluation is described.

*Biometric performance evaluation.* Commonly, a biometric system operates either in verification or identification mode and the term recognition is used universally.

For verification the system compares a query template to just one template of the biometric system database which is specified by the claimed identity of the query template. Consequently, the system accepts or rejects the claimed identity of

the individual/ object which results in 1:1 comparison. In case of identification a query template is compared to all templates in the database (1:N comparison). The system has to decide if the query template corresponds to an individual/ object which is enrolled in the system and furthermore it has to select a single template in the database that specifies the identity of the query template.

Generally, a biometric system is assessed based on the errors it produces [16]. Two major verification system errors (False Match Rate (FMR) and False Non Match Rate (FNMR)) result from the calculation of the intra- and interclass SDs which are commonly denoted as genuine and impostor SD, respectively. The intraclass SD contains all MSs computed between a set of templates of the same individual. The interclass SD contains the MSs between templates of different individuals. Consequently, the FMR includes all MSs between different individuals which are incorrectly accepted by the system. On the other hand the FNMR gives the proportion of MSs which were rejected although the score is computed between templates of the same individual. In the Receiver Operating Characteristic (ROC) curve the FMR/FNMR are plotted with respect to the system threshold. The ROC is typically used to measure the verification performance of a biometric system. Thereby, the equal error rate (EER) denotes the threshold where FMR and FNMR are equal. The EER is a general benchmark for the evaluation of biometric systems.

The performance of an identification system is evaluated by matching a set of probe templates to all templates enrolled in the database [10]. We refer to closed-set identification where it is assumed that all individuals/objects of the probe templates are enrolled in the system. The MSs between each probe template and all database templates are ordered according to the MS. The ordered MSs of each probe template are used to compute the probability that the correct template is ranked within the top  $k$ -ranked MSs. The probabilities for each rank are illustrated in a curve which is denoted as Cumulative Match Characteristic (CMC).

*Wood log cross-section variability.* Two basic requirements for biometric recognition are uniqueness and permanence of the utilized biometric characteristic. Uniqueness expresses that the biometric characteristic and the computed templates of different individuals are strongly varying and permanence is the requirement that they do not change over time. Related to those requirements there are two basic issues which a biometric system must handle: Intra-class variability and Interclass similarity. Interclass similarity is the problem that different individuals eventually show up similar biometric characteristics. Intra-class variability is an issue due to internal and external caused variations between a set of templates of the same individual. External variations occur due to irregularities in the template generation procedure, e.g. different sensors or capturing environments. Furthermore, the visual appearance of the biometric characteristic is affected or modified by external influences, e.g. abrasion of fingerprints. Internal variations are eventually caused by an intrinsic modification or change of the biometric characteristic itself, e.g. temporal variations caused by the

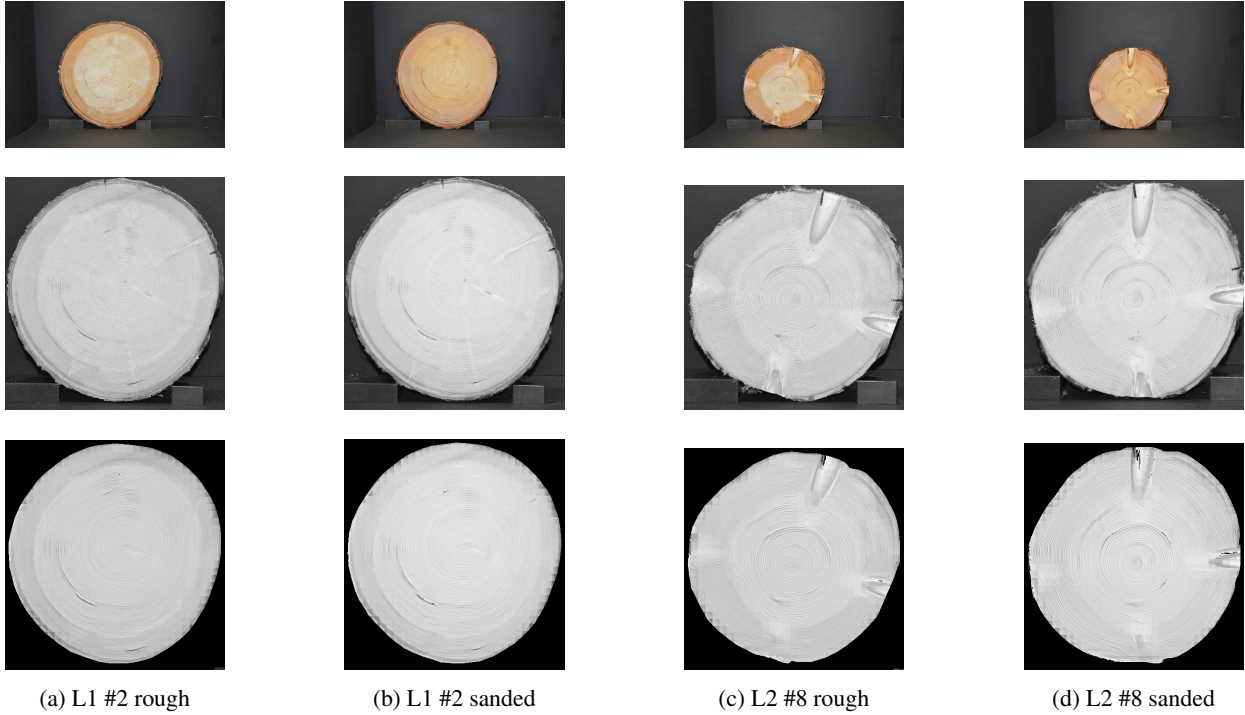


Figure 3: Testset examples: Slices #2 and #8 from L1 and L2, respectively. The CS-Images in the first row depict the original CS-Images and in row two and three the registered and enhanced CS-Images used for CS-Code computation are illustrated.

ageing process. In case of human biometrics, it is attempted to overcome external and internal changes/ modifications by updating the stored templates in the database.

In case of wood logs, several external and internal caused variations/ modifications of CSs of a single log have an impact on the intraclass variability. So far, three different variation types emerged from our research:

- **Temporal variations** correspond to the issue of ageing in human biometrics. In case of wood log ends, the visual appearance of a CS changes rapidly. Due to the rapidly changing moisture content at the front log side and the sun exposure the CS shows up discolourations or deformations (e.g. cracks). In Fig. 4 four time-delay captured CS-Images of a CS-Slice from L3 illustrate temporal variations.



Figure 4: Temporal variations of CS-Slices: Slice #10 - Section 2 / Sessions 1-4 [19]

- **Longitudinal variations** are caused by the changing CS pattern along the longitudinal axis of a single tree log. Consequently, they address the issue of length-cutting a log in the sawmill. An illustration for longitudinal variations of the CSs from a single log is presented in Fig. 5.



Figure 5: Longitudinal variations: L2 - Slices #1, 4, 8, 16

- **Surface variations** result from differently finished or cut surfaces of a particular CS. In this work surface variations between saw cut CS surfaces and the sanded CS surface counterparts are assessed (e.g. see Fig.3). Another scenario which is closely related to industrial biometric log recognition involves CS surface variations caused by different cutting tools (e.g. chain-, band- or circular saw). Probably the first cut in the forest and the cleansing cut in the sawmill are performed with different devices. This results in a mixture of longitudinal and surface variations.

For the testset CS-Images of the CS-Slices from L1,L2 and L3 we tried to avoid external variations which are caused by the capturing procedure.

*Intra-/Interclass score distributions (SDs).* For the evaluation, the MSs between all CS-Images of L1,L2 and L3 are computed using the proposed matching procedures. The inter-/interclass SDs for a single matching procedure are constructed by grouping the MSs into the respective SD. Hence, the interclass SD contains all MSs computed between the CS-Images of L1,L2 and L3. The intraclass SD is build up on the MSs between CS-Images of the same log and is further subdivided into two SD

groups corresponding to the variation type (see Table 2). Temporal variations which are represented by the MSs between the four time-delay captured CS-Images of each CS-Slice from L3 were investigated in [19] and are not treated in this work. The longitudinal SD describes the similarity between CS-Images which were captured at different longitudinal positions of the same log. In this work we consider the longitudinal variations of L1 and L2. For this purpose, the longitudinal SD is built up on the MSs between the CS-Images of rough or sanded CS-Slices from L1 and L2. The surface SD includes all MSs between the saw cut CS surfaces and the sanded CS surface counterparts of each CS-Slice from L1 and L2.

Intraclass SD	
CS Variation	SD group details
Longitudinal SD	L1&L2: MSs between the rough or sanded CS-Images of their CS-Slices
Surface SD	L1&L2: MSs between the rough and sanded CS-Image of each CS-Slice

Table 2: Intraclass SD groups

### 3. Results and Discussion

The results of the experiments are subdivided into two sections. Section 3.1 presents investigations on the separability of the intra- and interclass SDs. For this purpose, the verification performance of the biometric system for different matching procedures is assessed and the EERs are considered. Because of the manifold structure of the intraclass SD an exhaustive analysis of the longitudinal and surface SD group is presented. Based on the results, fundamental conclusions on the intraclass variability and the impact on the separability between intra- and interclass SDs are drawn.

Section 3.3 treats the identification performance for different real world scenarios. Introductory, the gathered insights of Section 3.1 are summarized and the cumulative matching score ranks of the intraclass SD groups and the interclass SD are analysed.

#### 3.1. Intra-/Interclass SD separability

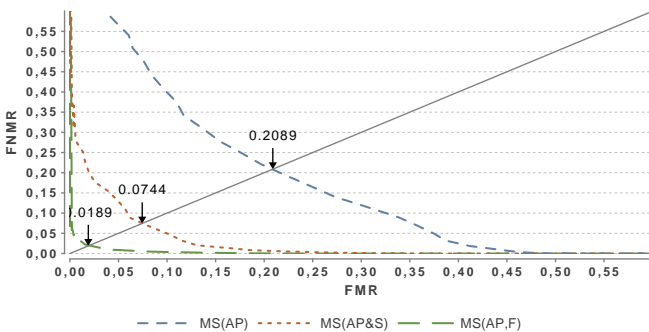


Figure 6: Equal Error Rates (EER) for different matching procedures

Of course, the interclass SD is just built-up on three individuals, but the results give first important and fundamental insights

on the applicability of biometric log recognition using log end images. As described in Section 2.3 three different matching procedures are assessed. In Fig.7 the intra-/interclass SDs for each particular matching procedure are illustrated. Due to the unequal cardinality of the intra-/interclass SDs they are normalized according to their cardinalities. Most important, the three charts indicate that the shape of a CS is a valuable biometric feature. Compared to the  $MS_{AP}$  intra-/interclass SD, the SD overlap decreases remarkably for the  $MS_{AP\&S}$  and  $MS_{AP,F}$  matching procedures. The results for  $MS_{AP}$  which just rely on the discriminative power of the annual ring pattern show a high overlap between the intra-/interclass SDs.

In Fig. 6 the receiver operator curve (ROC) illustrates the FMR/FNMR ratios with respect to the system threshold. The EER for  $MS_{AP}$ , which accounts  $\sim 21\%$  is insufficient for any biometric system. By including shape information in the matching procedure ( $MS_{AP\&S}$ ) the EER can be pushed down to  $\sim 7\%$ . The lowest EER is achieved using the score level fusion matching procedure ( $MS_{AP,F}$ ) with an EER of approximately  $\sim 2\%$ . Our experiments in [19] showed that the similarity between different CS-Slices of a log deteriorates with an increasing distance between the considered CS-Slices. Hence, an EER of  $\sim 2\%$  is astonishing because the intraclass SD includes all longitudinal MSs for all slice distances. A detailed analysis of the considered intraclass SD groups (Longitudinal and Surface SD) allows to draw more detailed conclusions.

#### 3.2. Intraclass SD analysis

In this section the longitudinal SD and surface SD groups of which the intraclass SD is build up are assessed in detail.

##### 3.2.1. Longitudinal SD

The longitudinal SD contains the MSs between the rough or sanded CS-Images of the CS-Slices from L1 and L2. In the evaluation four subsets of the longitudinal SD are assessed: Rough & Sanded longitudinal MSs of L1 and L2. Furthermore, the MSs of each subset are grouped according to their neighbourhood distance of the compared CS-Slices. In case of 16 CS-Slices for each log the distances range from 1 to 15 and consequently 15 slice distance groups (SDGs) are considered. For example, SDG 1 contains all MSs of each CS-Slice to its adjacent neighbour CS-Slices. In Fig. 8 for all matching procedures the mean values of each subset and SDG are depicted.

Independent of the subset and matching procedure it is expected that the longitudinal MSs increase the higher the slice distance between two CS-Slices is. Previously, in [19] our experiments based on CS-Slices from L3 confirmed this expectation. At a glance, the results for all matching procedures shown in Fig. 8 raise doubt on the correctness of the previous results and the basic assumption.

Considering the longitudinal MSs of the first log (Sanded#1, Rough#1) the expected increase is interrupted for both subsets and matching procedures. This interrupt is also shown for the second log (Sanded#2, Rough#2) for the SDGs 14,15. A closer examination of the CS-Slices of L1,L2 and L3 provides an answer for the differing results. For L3 just the CS-Slices at the

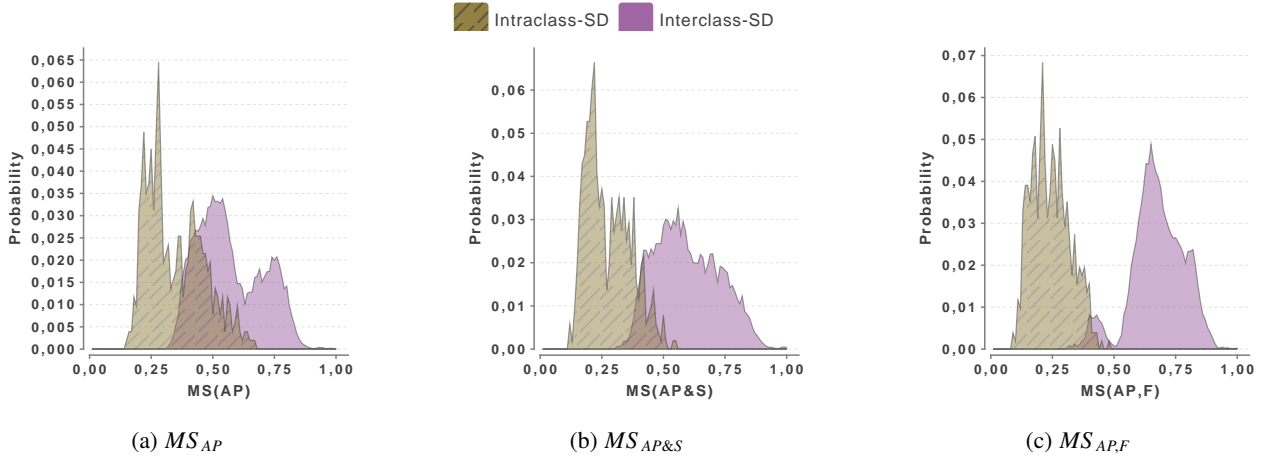


Figure 7: Intra-/Interclass score distributions (SD) for different matching procedures

log ends show up knots. Hence, for larger distances the longitudinal MSs increase additionally and the expected trend becomes strengthened. In contrast to this, L1 and L2 show up knotty CS-Slices situated in the middle of each log. For L1 one (#9 see Fig. 3d) and for L2 two CS-Slices (#10,#11) show up 4 knots. By omitting MSs from those knotty CS-Slices the results in Fig. 9 approximately show the expected behaviour. This leads to two major conclusions. Less surprising, the results demonstrate that MSs between non-knotty (NK) and knotty CS-Slices are remarkably worse. Second, the results indicate that knots do not introduce any propagative effects to the annual ring pattern.

In comparing the results from L1 to L2 it is clearly visible that the MS ranges of the longitudinal MSs of different logs vary. Particularly for higher slice distances, this effect is shown in Fig. 9 and Fig. 8 where the gaps between the subsets of both logs tear up significantly. However, it can be stated the longitudinal MSs of each log are increasing with the slice distance.

### 3.2.2. Longitudinal SD/ Interclass fractions

The longitudinal increase of the MSs leads to the conjecture that for higher slice distances it is not possible to separate be-

tween longitudinal MSs and interclass MSs. This conjecture is validated by considering the interclass fraction of the longitudinal MS-SDGs. The interclass fraction of a SDG is specified as the percentage the SDG MSs which intersect with the interclass SD. In considering the interclass fractions of the SDGs of different longitudinal MSs conclusions about the separability can be drawn. For this purpose, the interclass fractions of each SDG and longitudinal SD subset with the interclass SD are computed and illustrated in Fig. 10. All results for L1 show that by ignoring the knotty CS slices nearly no MSs are in the range of the interclass SD. Completely different, the longitudinal MSs of L2 computed with  $MS_{AP}$  and  $MS_{AP\&S}$  significantly overlap with the interclass SD. This applies to the knot-slice excluding subsets of L2 too and indicates that the intrinsic features (annual ring pattern) of L2 change quite rapidly. The smallest overlaps for L1 and L2 are computed with the  $MS_{AP,F}$  matching procedure. The non-knot subsets of L1&L2 and the SDGs 1,2 do not overlap with the interclass SD. Hence, a more sophisticated matching procedure which uses shape information is more robust to a higher intrinsic change of the annual ring pattern of a log.

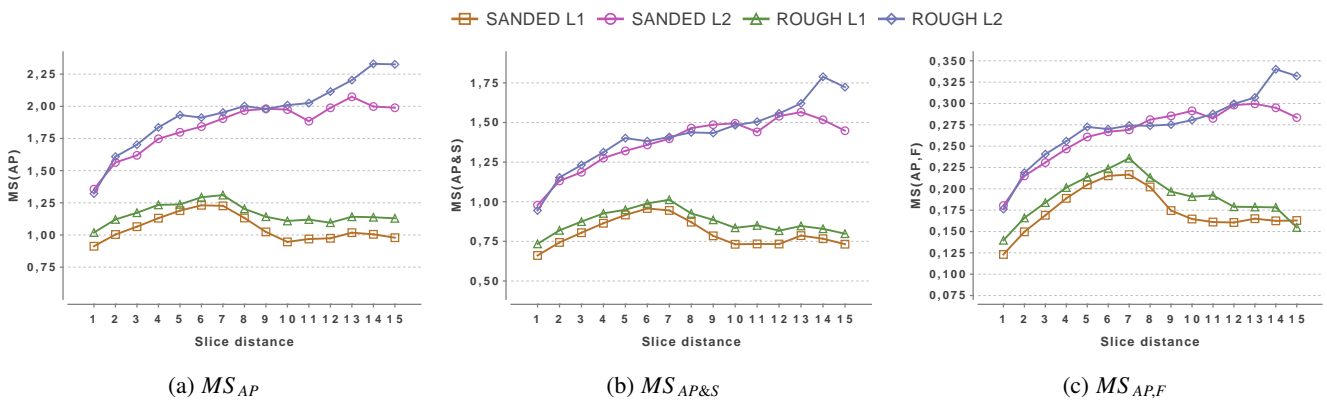


Figure 8: Intraclass SD: Rough and Sanded longitudinal MSs of L1 and L2 grouped by the slice distance.

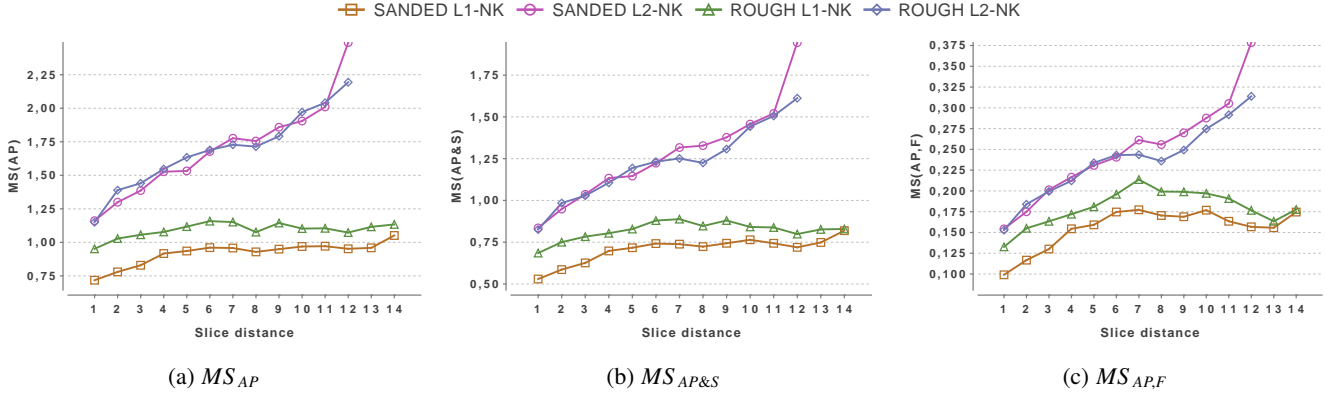


Figure 9: Longitudinal variance analysis excluding knotty CS-Slices - L1(#9), L2(#10,#11)

### 3.2.3. Surface SD

The surface SD is examined in context of the previously analysed longitudinal SD subsets and the interclass SD. Again, the main objective is to assess the separability between the surface SD subsets and the interclass SD. In case of the CS-Images of L1 and L2 the surface MSs are the only MSs between CS-Images from equal CS-Slices. The surface MSs between the rough and sanded CS-Images are considered for L1 and L2, separately. For all SDs the cumulative distribution functions (CDF) are computed and illustrated for each matching procedure (see Fig. 11). The CDF for each SD gives the probability that a certain MS exists that is ranged less or equal to that MS. Furthermore, the CDF illustrates the mean value (Probability = 0.5) and the variance range of each SD. Hence, the CDFs of a certain intraclass SD group/subset and the interclass SD can be used to observe their overlap and to draw conclusions about their separability.

Generally, it is expected that the CDFs of the surface SD subsets are ranged below the longitudinal SD CDFs. As shown for the longitudinal SD subsets of L1 & L2, the MS ranges of the surface SD subsets of L1 and L2 vary too. For L1 and all matching procedures the CDF of the Surface-RoughSanded-L1 subset does not overlap with the interclass CDF. In case of the Longitudinal-L1 CDFs low overlaps are visible which are caused by the longitudinal increase of the MSs. The

largest overlaps with the interclass CDFs are shown for the Longitudinal-L2 CDF subsets. Especially, for  $MS_{AP}$  this overlap is clearly visible. These overlaps are responsible for the large overlaps between the intra-/intraclass SDs in Fig. 7 for the  $MS_{AP}$  and  $MS_{AP\&S}$  matching procedures. Again, the Longitudinal-L2 CDF of  $MS_{AP,F}$  illustrates that this overlap can be reduced by utilizing shape information.

Surprisingly, for  $MS_{AP}$  and  $MS_{AP\&S}$  the Surface-RoughSanded-L2 CDFs also overlaps with the interclass CDFs. By inspecting the enhanced images of the CS-Images from L2 it was obvious that these overlaps are caused by two CS-Images for which the utilized enhancement procedure fails and deteriorates parts of the annual ring pattern.

### 3.3. Identification performance

So far, all evaluations were related to the verification performance biometric log recognition using log end images. Based on the gathered insights, two investigations on the identification performance are presented.

First, the MSs for each CS-Slice of L1 and L2 are ordered and the ranks for different intraclass groups/subsets MSs and the interclass MSs are analysed. Hence, global statements on the rank orders can be presented.

Second, the identification rates for four specific identification scenarios are presented. All scenarios illustrate the im-

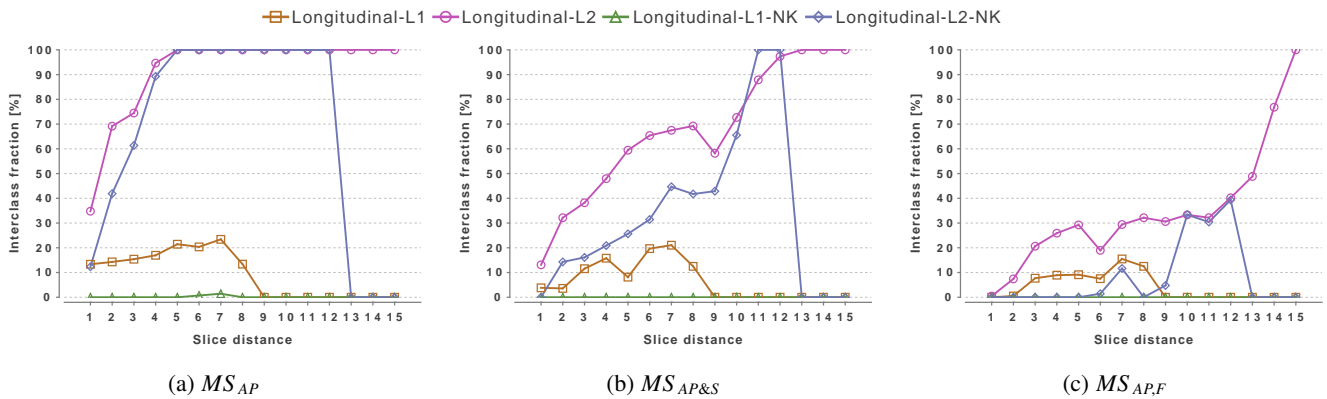


Figure 10: Relative longitudinal/interclass overlaps for the slice distance groups (SDGs) of each longitudinal SD subset

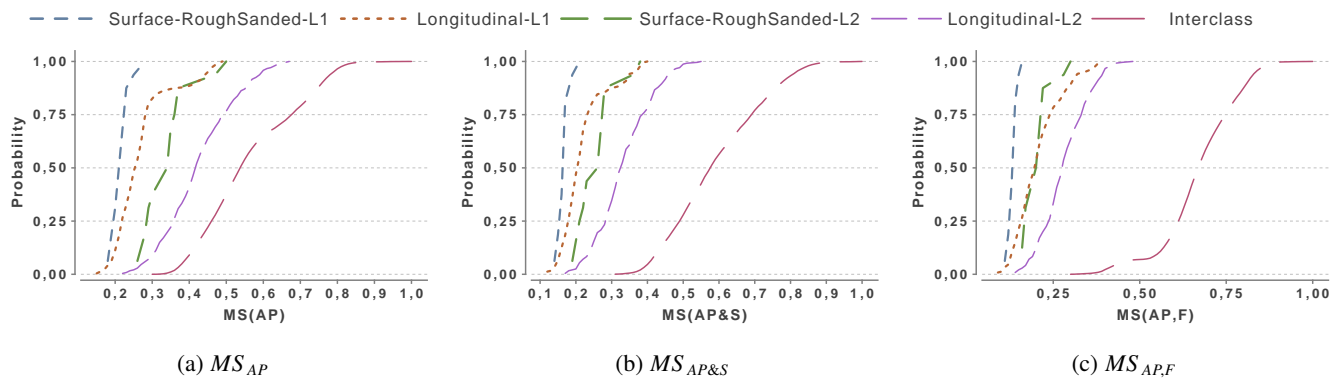


Figure 11: Cumulative distribution functions (CDFs) for different longitudinal and surface SD subsets and the interclass SD

pect of cutting the log end on the identification performance. Thereby, it is elaborated how the width of the piece which is cut-off influences the performance. Furthermore, the impact of using different cutting tools is assessed.

### 3.3.1. Cumulative CS-Slice matching score ranks

Commonly, the CMC depicts how the biometric system ranks the MSs of a set of probe templates compared to the database templates. For this investigation the CMC is used to illustrate the MS ranks of five intraclass SD groups/subsets and the interclass SD.

For this purpose, all MSs between the templates of the CS-Images of each CS-Slice to all other templates in the database are ordered with respect to the MS. For the CMC, the probability of observing a MS belonging to a certain SD in the first  $k$ -ranks is determined and visualized for all matching procedures in Fig. 12.

The intraclass SD group SURFACE shows the detection rates for the MSs between rough and sanded CS-Images of each CS-Slice. For the four longitudinal SD group subsets just MSs for slice distance group 1 or 2 are considered. The CMC curves of these longitudinal SD subsets illustrate the robustness of the biometric system against longitudinal variations of the CS (e.g. cutting the log end once or twice).

In comparing the CMC curves for the intraclass SD

groups/subsets to the interclass SD CMC curve we can draw first conclusions on the identification performance of the biometric system. Most important, for all matching procedures and CS-Slices each considered intraclass SD group/subset shows up high detection rates at the best (=lowest) ranks. On the other hand, the probability of observing a well ranked ( $\leq 10$ ) interclass SD-MS is very low. In case of  $MS_{AP,F}$  nearly all intraclass SD-MSs are ranked in front of the first interclass SD-MS occurrence. In comparing the surface SD ranks to the longitudinal SD subset ranks the results confirm the conclusions of the longitudinal SD analysis. Surprisingly, the MSs of the rough and sanded longitudinal SDs of L1 are ranked in front of the surface SD-MSs. Furthermore, the MSs of the rough and sanded longitudinal SDs of L2 are ranked in the range of the surface SD-MS. This leads to the assumption that CS-Images of adjacent neighboured CS-Slices with equal surfaces show up a higher or almost equal similarity to each other than the rough and sanded CS-Images of the CS-Slices. Again, the results depict the high longitudinal CS variability of L2 which is demonstrated by the higher ranked MSs for the longitudinal SD subsets of L2.

Most important, the results show that the first occurrence of an interclass MS is worse ranked (= high ranked). The interclass CMC curves for  $MS_{AP}$ ,  $MS_{AP,F}$  illustrate that by including shape information the interclass detection rates shift remarkably to higher ranks.

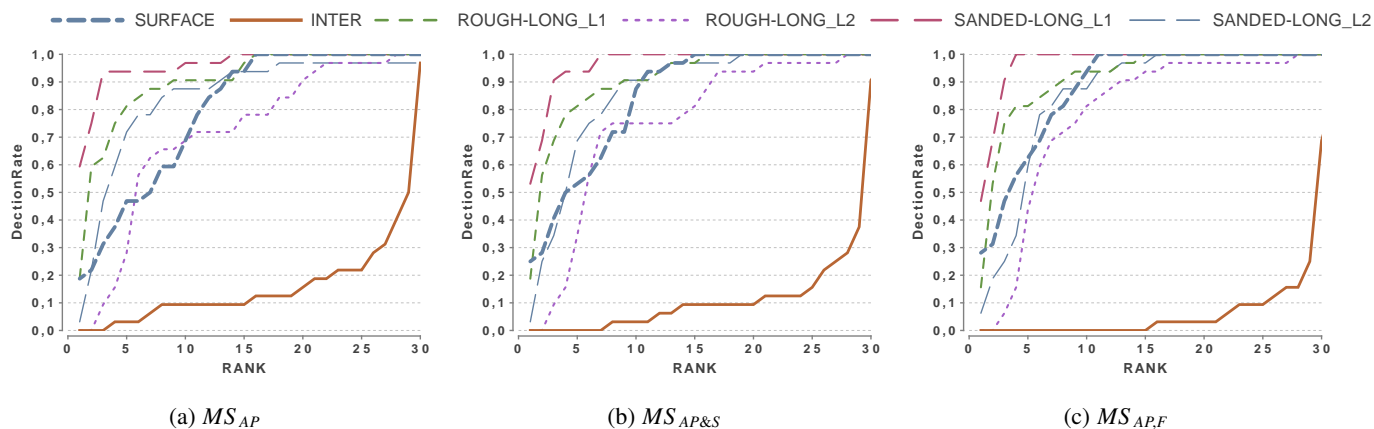


Figure 12: Cumulative matching score ranks

### 3.3.2. Identification performance - Test scenarios

Finally, the identification performance for different scenarios is assessed. A test scenario requires to specify a probe set and a gallery set. The gallery specifies the enrolled templates of the individuals/objects contained in the database. The probe set is a set of templates of individuals/objects which are used to query the biometric system. For each probe template the matches/MSs to all database templates are computed. The computed matches/MSs for each probe template are ordered and the rank of the correct match/MS is determined. Subsequently, for each rank the probability that the correct match/MS is equal or better ranked is computed. For illustration these probabilities are depicted in a CMC chart. The probability that the correct match is ranked at the first position is denoted as identification rate or detection rate. Basically, all scenarios evaluate the impact of cutting the log end in the sawmill.

*Scenario #1,#2 - Equal CS-Surfaces.* For these scenarios it is assumed that the first cut in the forest and the second cut in the sawmill is performed with the same cutting tool. Hence, no surface variations due to different cutting tools are introduced. For this purpose Scenario #1 (Rough-Rough) is based on rough CS-Images and Scenario#2 (Sanded-Sanded) is based on sanded CS-Images of L1 and L2. As probe templates for Scenario#1,#2 the rough or sanded CS-Images of each CS-Slice are utilized, respectively. For each scenario and probe template it is assumed that just one equal surfaced CS-Image of the same log which belongs to a certain slice distance group (SDG) is enrolled in the gallery set. For the evaluation SDGs ranged between 1 and 5 are considered. Furthermore, templates of all CS-Images from L3 and equal surfaced CS-Images of the other log (L1 or L2) are included in the gallery. For each probe template the rank of the correct match is computed and in Table 3 the results for both scenarios are summarized. For each scenario the identification rates for different SDGs and matching procedures are illustrated. Because of the high identification rates, a graphical illustration in a chart is less meaningful.

In comparing the results of Scenario#1 and #2 it is recognizable that the identification rates for all matching procedures are

Rough-Rough					
MP/SDG	1	2	3	4	5
$MS_{AP}$	1.0	0.94	0.88	0.81	0.72
$MS_{AP\&S}$	1.0	1.0	0.91	0.88	0.81
$MS_{AP,F}$	1.0	1.0	0.97	0.94	0.91
Sanded-Sanded					
MP/SDG	1	2	3	4	5
$MS_{AP}$	0.97	0.97	0.91	0.84	0.81
$MS_{AP\&S}$	1.0	0.97	0.97	0.88	0.84
$MS_{AP,F}$	1.0	1.0	0.97	0.97	0.88

Table 3: Scenario#1,#2 - Identification rates for different slice distance groups (SDGs) and matching procedures (MPs)

somewhat equal. Consequently, the CS-Surface has no impact on the identification performance of Scenario#1 and #2. For  $MS_{AP,F}$  and the SDGs 1,2 the identification rates account 100%. This indicates that the biometric system is robust to cutting the log end in a range of five centimetres (2 CS-Slices = 5cm). Additionally, the results illustrate that for higher SDGs shape information is beneficial to increase the identification rate. Depending on the matching procedure the rates for higher SDGs are still in a range between 72% and 97%.

*Scenario #3,#4 - Different CS-Surfaces.* In difference to the first two scenarios, Scenario #3 and #4 investigate the impact of different surfaced CSs. Thus, it is assumed that the first cut in the forest and the second cut in the sawmill are performed with different cutting tools. Based on the CS-Images of L1 and L2 two scenarios are constructed. Scenario #1 (Rough-Sanded) assumes that the first cut is represented by a rough CS-Image of a CS-Slice and the second cut is represented by a sanded CS-Image of a neighbored CS-Slice. Scenario #2 (Sanded-Rough) assumes that the cuts are performed in the reverse order. Consequently, these scenarios result in a mixture of longitudinal and surface CS variations. For both scenarios the rank-orders for the correct matches are computed in the same way as for the first two scenarios. The CMC curves for each scenario, matching procedure and SDG are illustrated in Fig. 13 and Fig. 14. The results for Scenario #3 in Fig. 13 illustrate that for all matching procedures the identification performance decreases remarkable for higher SDGs. Compared to Scenario#1 and #2,

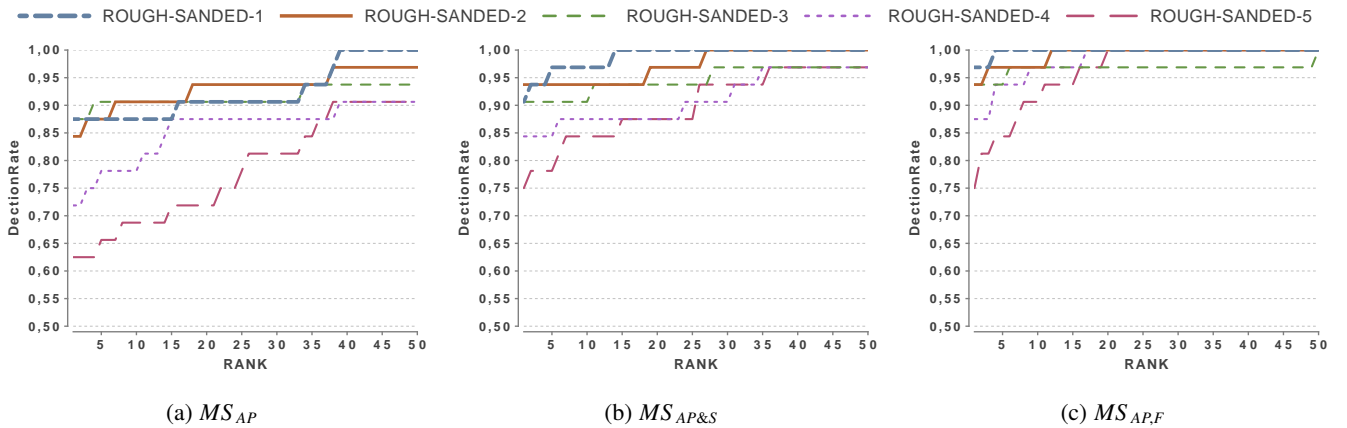


Figure 13: Scenario #3: Identification performance for different CS-Surfaces with respect to the width which is cut off from the log end (Enrolled set: Rough CS-Images, Probe set: Sanded CS-Images from different SDGs)

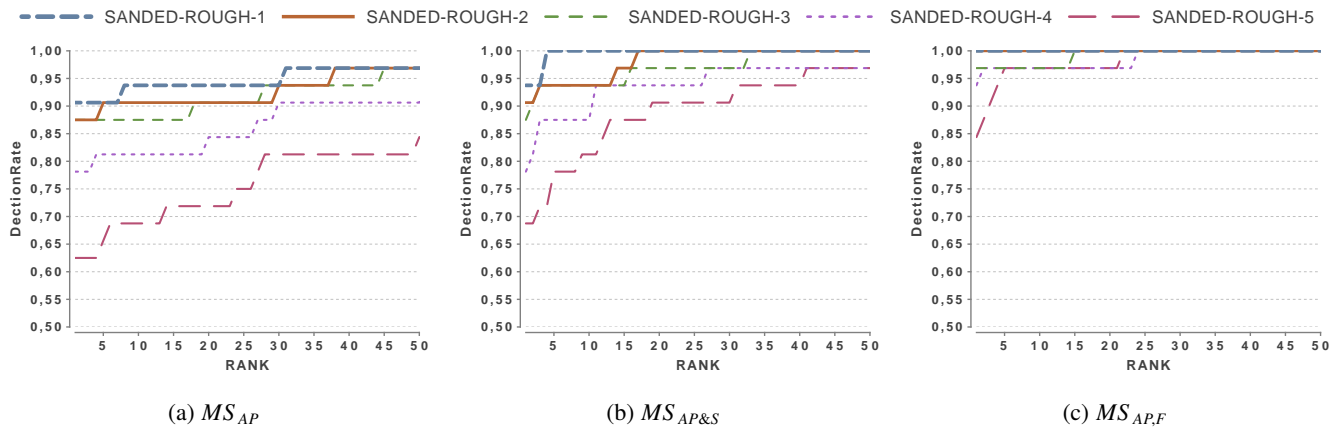


Figure 14: Scenario #4: Identification performance for different CS-Surfaces with respect to the width which is cut off from the log end (Enrolled set: Sanded CS-Images, Probe set: Rough CS-Images from different SDGs)

the identification rates (Rank 1) are considerably worse. Just for  $MS_{AP,F}$  and SDG 1 an identification rate of approximately 97% is reached. Generally, the results indicate that CS-Surface variations cause a remarkable decrease of the identification performance. Finally in Fig. 14 the results for Scenario#4 are shown. For almost all depicted CMC curves the identification performance is better than for Scenario #3. For  $MS_{AP,F}$  and SDG 1,2 the identification rate accounts 100% and is above 93% for SDG 3 and 4. However, the results for all scenarios indicate that biometric log recognition using log end images is robust to longitudinal variations and mixtures of surface and longitudinal variations to a certain degree. Furthermore, all evaluations showed that shape information are valuable to increase the discriminative power of the biometric system.

#### 4. Conclusions

The findings of this study demonstrate that biometric features extracted from wood log cross-sections are suited to discriminate between different tree logs in an industrial application. It can be concluded that the robustness of the biometric system to CS variations depends on the template computation approach and the utilized matching procedure.

In comparing the results for three different matching procedures it is obvious that biometric feature fusion increases the robustness significantly. Regarding to the verification performance, a combination of annual ring pattern and shape features increases the robustness to longitudinal CS variations. Furthermore, the analysis of the intraclass SD groups illustrates that CS surface variations are not crucial for the biometric performance.

Based on the identification performance experiments we conclude that biometric log recognition is qualified to overcome the issue of cutting log ends in the sawmill. Results show a successful identification within cutting off slices up to ~7.5 centimeters in thickness, even if the second cut in the sawmill is performed with another cutting tool.

The analysis of the longitudinal CS variations for different slice distances points out that knots are disturbing factors. This is caused by the fact that the current approach is not dealing

with knots on CSs. Surprisingly, the results indicate that knots do not introduce any propagative effects to the annual ring patterns. Thus, future work should investigate the similarity between non-knotty parts of knotty CSs and their neighbored knot free CSs.

Although the results of this study are based on slices from three different tree logs, further experiments on a large set of tree logs are indispensable to assess the identification performance in a real world environment. Furthermore, the applicability of other feature extraction methods should be assessed and new log template computation approaches and matching procedures should be developed. Finally, further research should deal with the impact of automatic pith estimation and CS segmentation approaches to the biometric system performance.

#### 5. Literature cited

- [1] Chiorescu, S., Grönlund, A., 2003. The fingerprint approach: using data generated by a 2-axis log scanner to accomplish traceability in the sawmill's log yard. *Forest Products Journal* 53, 78–86.
- [2] Chiorescu, S., Grönlund, A., 2004. The fingerprint method: Using over-bark and under-bark log measurement data generated by three-dimensional log scanners in combination with radiofrequency identification tags to achieve traceability in the log yard at the sawmill. *Scandinavian Journal of Forest Research* 19, 374–383.
- [3] Dykstra, D.P., Kuru, G., Taylor, R., Nussbaum, R., Magrath, W.B., Story, J., 2003. Technologies for Wood Tracking. Technical Report. World Bank - WWF Alliance report.
- [4] EuropeanParliament, 2010. Regulation (EU) No 995/2010 of the European Parliament and of the council of 20th October 2010 laying down the obligations of operators who place timber and timber products on the market.
- [5] Flodin, J., Oja, J., Grönlund, A., 2007. Fingerprint traceability of sawn products using x-ray log scanning and sawn timber surface scanning, in: *Proceedings of Quality control for wood and wood products: COST Action E 53 the first conference*.
- [6] Flodin, J., Oja, J., Grönlund, A., 2008a. Fingerprint traceability of logs using the outer shape and the tracheid effect. *Forest Products Journal* 58, 21–27.
- [7] Flodin, J., Oja, J., Grönlund, J., 2008b. Fingerprint traceability of sawn products using industrial measurement systems for x-ray log scanning and sawn timber surface scanning. *Forest Products Journal* 58, 11.
- [8] Hong, L., Wan, Y., Jain, A., 1998. Fingerprint image enhancement: Algorithm and performance evaluation. *IEEE Trans. Pattern Anal. Mach. Intell.* 20, 777–789.

- [9] Jain, A., Ross, A., Prabhakar, S., 2001. Fingerprint matching using minutiae and texture features, in: *Procs. of the International Conference on Image Processing (ICIP'01)*, Thessaloniki, GR. pp. 282–285.
- [10] Jain, A.K., Flynn, P., Ross, A.A., 2007. *Handbook of Biometrics*. Springer-Verlag New York, Inc., Secaucus, NJ, USA.
- [11] Jain, A.K., Prabhakar, S., Hong, L., Pankanti, S., 2000. Filterbank-based fingerprint matching. *IEEE Transactions on Image Processing* 9, 846–859.
- [12] Jain, A.K., Ross, A.A., Nandakumar, K., 2011. *Introduction to Biometrics*. Springer US.
- [13] Kastner, T., Erb, K.H., Nonhebel, S., 2011. International wood trade and forest change: A global analysis. *Global Environmental Change* 21, 947–956.
- [14] Knutsson, H., Granlund, G.H., 1983. Texture analysis using two-dimensional quadrature filters, in: *IEEE Computer Society Workshop on Computer Architecture for Pattern Analysis and Image Database Management*, Pasadena, USA.
- [15] Kuemmerle, T., Chaskovskyy, O., Knorn, J., Radeloff, V.C., Kruhlov, I., Keeton, W.S., Hostert, P., 2009. Forest cover change and illegal logging in the ukrainian carpathians in the transition period from 1988 to 2007. *Remote Sensing of Environment* 113, 1194–1207.
- [16] Maltoni, D., Maio, D., Jain, A.K., Prabhakar, S., 2009. *Handbook of fingerprint recognition*. Springer New York.
- [17] Norell, K., Borgfors, G., 2008. Estimation of pith position in untreated log ends in sawmill environments. *Computers and Electronics in Agriculture* 63, 155–167.
- [18] Richards, M., Wells, A., Del Gatto, F., Contreras-Hermosilla, A., Pomnier, D., 2003. Impacts of illegality and barriers to legality: a diagnostic analysis of illegal logging in honduras and nicaragua. *International Forestry Review* 5, 282–292.
- [19] Schraml, R., Charwat-Pessler, J., Uhl, A., 2014. Temporal and longitudinal variances in wood log cross-section image analysis, in: *IEEE International Conference on Image Processing 2014 (ICIP 2014)*, Paris, FR.
- [20] Schraml, R., Uhl, A., 2013. Pith estimation on rough log end images using local fourier spectrum analysis, in: *Proceedings of the 14th Conference on Computer Graphics and Imaging (CGIM'13)*, Innsbruck, AUT.
- [21] Smith, J., Obidzinski, K., Subarudi, Suramenggala, I., 2003. Illegal logging, collusive corruption and fragmented governments in kalimantan, indonesia. *International Forestry Review* 5, 293–302.
- [22] Tzoulis, I., Andreopoulou, Z., 2013. Emerging traceability technologies as a tool for quality wood trade. *Procedia Technology* 8, 606–611.
- [23] United Nations, 1992. United nations conference on environment & development, in: *Agenda 21*, Rio de Janeiro, BR.